Van Hove Singularities in the Quark-Gluon Plasma

Markus H. Thoma[a*]

[a]Theory Division, CERN, CH-1211 Geneva 23, Switzerland

General arguments as well as different approximations for the in-medium quark propagator in a quark-gluon plasma lead to quark dispersion relations that exhibit a minimum in one branch (plasmino). This minimum causes Van Hove singularities in the dilepton production rate and mesonic correlators, which might have observable consequences.

1. Introduction

In 1953 Van Hove [1] discussed singularities in the density of states, so-called Van Hove singularities, in solid state physics. The density of states of a system, given by

$$g(\omega) = \sum_n \int \frac{\mathrm{d}^3k}{(2\pi)^3}\, \delta(\omega - \omega_n(\boldsymbol{k})) \tag{1}$$

with the energy eigenstates $\omega_n(\boldsymbol{k})$, can be expressed by the surface integral [2]

$$g(\omega) = \sum_n \int \frac{\mathrm{d}S}{(2\pi)^3}\, \frac{1}{|\nabla\omega_n(\boldsymbol{k})|}. \tag{2}$$

Here the quantity in the denominator $|\nabla\omega_n(\boldsymbol{k})|$ can be identified with the group velocity. Due to symmetries in a crystal the group velocity vanishes at certain momenta, resulting in a divergent integrand in (2). This divergence is integrable in 3 dimensions, leading to a finite density of states. In lower dimensions, however, Van Hove singularities appear. For example, a 2-dimensional electron gas shows logarithmic singularities, which have been discussed in connection with high-T_c superconductors [3].

Here we want to discuss the role of Van Hove singularities in a quark-gluon plasma. We will argue that the in-medium quark dispersion relation consists of two branches of which one has a minimum at some finite value of the momentum. This leads to a vanishing group velocity for the collective quark modes. Interesting quantities such as the production rate of low mass lepton pairs and mesonic correlators depend inversely on this group velocity. Therefore these quantities, which follow from self energy diagrams containing a quark loop, are affected by Van Hove singularities, which might have observable consequences.

In the next two sections we will show the origin of Van Hove singularities using an effective quark propagator for the quark loop in the self energies under consideration. First we will use the so-called hard thermal loop (HTL) resummed quark propagator. After that we discuss the implications of a quark propagator considering the presence of a non-vanishing gluon condensate in the deconfined phase as indicated by lattice QCD calculations. In section 4 we will argue that the minimum in the quark dispersion relation and thus the appearance of Van Hove singularities is a general property of massless fermions at finite temperature. Finally we will discuss the chances and problems to observe Van Hove singularities and to prove in this way the presence of deconfined collective quarks in relativistic heavy ion collisions.

2. Hard thermal loop approximation

The HTL resummation technique has been developed by Braaten and Pisarski to cure some serious problems of perturbation theory for gauge theories at finite temperature [4]. Using only bare propagators and vertices naive perturbation theory lead to gauge dependent and infrared divergent results for physical quantities. A famous ex-

*Heisenberg Fellow

ample is the damping rate of a long-wave, collective gluon mode in the QGP, which was found to depend on the gauge choice and became even negative corresponding to a plasma instability in covariant gauges [5]. Braaten and Pisarski realized that this undesirable behaviour is due to the fact that higher order loop diagrams contribute to lower order in the coupling constant at finite temperature. Distinguishing between a soft momentum scale gT, where g is the gauge coupling, and a hard scale of order T, Braaten and Pisarski isolated the dangerous diagrams. They are given by one-loop self energies and vertices, which contain only hard loop momenta and are related to each other by Ward identities. For example, in the case of the polarization tensor in QED or QCD a result proportional to g^2T^2 was obtained[2]. Resumming these self energies and vertices within the Dyson-Schwinger equation effective propagators and vertices can be constructed. These effective Green functions have to be used if all legs of the Green function under consideration are soft. Otherwise bare propagators and vertices are sufficient. Physical quantities calculated by applying this HTL improved perturbation theory, such as the gluon damping rate [8], turn out to be gauge invariant. At the same time medium effects such as Debye screening, leading to an improved infrared behaviour, and Landau damping are included. For a review of the HTL resummation method and its applications to the physics of the QGP see Ref.[9].

Let us now consider the HTL approximation for the quark propagator in the QGP. Assuming that the temperature is much larger than the mass, which holds at least for up and down quarks, we can neglect the quark masses. Then the most general expression for the fermion self energy in the heat bath can be written as [10]

$$\Sigma(K) = -a(k_0,k)K^\mu\gamma_\mu - b(k_0,k)\gamma_0, \qquad (3)$$

using the notation $K \equiv (k_0, \boldsymbol{k})$, $k \equiv |\boldsymbol{k}|$. The scalar quantities a and b are functions of the energy k_0 and magnitude k of the three momentum. They are given by traces over the self energy

$$a(k_0,k) = \frac{1}{4k^2}\left[tr(K^\mu\gamma_\mu\,\Sigma) - k_0\,tr(\gamma_0\,\Sigma)\right], \quad (4)$$

$$b(k_0,k) = \frac{1}{4k^2}\left[K^2\,tr(\gamma_0\,\Sigma) - k_0\,tr(K^\mu\gamma_\mu\,\Sigma)\right],$$

which read in the HTL approximation

$$\begin{aligned} tr(K^\mu\gamma_\mu\,\Sigma) &= 4\,m_q^2\,, \\ tr(\gamma_0\,\Sigma) &= 2\,m_q^2\,\frac{1}{k}\,\ln\frac{k_0+k}{k_0-k} \end{aligned} \qquad (5)$$

with the effective thermal quark mass $m_q^2 = g^2T^2/6$. Note that the general ansatz (3) is chirally invariant in spite of the occurrence of an effective quark mass [10]. Furthermore the quark self energy has a non-vanishing imaginary part below the light cone ($k_0^2 < k^2$) which can be related to Landau damping for spacelike quark momenta.

For massless quarks it is convenient to decompose the quark propagator into its helicity eigenstates ($\hat{\boldsymbol{k}} = \boldsymbol{k}/k$) [11]

$$S(K) = \frac{\gamma_0 - \hat{\boldsymbol{k}}\cdot\boldsymbol{\gamma}}{2D_+(K)} + \frac{\gamma_0 + \hat{\boldsymbol{k}}\cdot\boldsymbol{\gamma}}{2D_-(K)}. \qquad (6)$$

The zeros $\omega_\pm(k)$ of

$$D_\pm = (1+a)\,(-k_0 \pm k) - b, \qquad (7)$$

describe the dispersion relation of the particle excitation q_+ with energy ω_+ and of a mode q_-, called plasmino [11], with energy ω_- and negative ratio of chirality to helicity. The latter is a consequence of the medium, breaking the Lorentz invariance of the vacuum.

The HTL quark dispersion relations are shown in Fig.1. We observe that both branches start at zero momentum at the same energy $\omega_\pm(0) = m_q$ and approach the bare dispersion $\omega = k$ at large momenta. The plasmino branch, which is absent in the vacuum, has a minimum at $k = 0.408\,m_q$. The spectral strength of the plasmino decreases exponentially for large momenta, indicating the purely collective nature of this mode.

The emission of thermal lepton pairs from the QGP proceeds via the decay of a virtual photon produced to lowest order by quark-antiquark annihilation. For low invariant masses of the order gT medium effects from the collective quark

[2]This result has been found before in the high temperature approximation [6] and much earlier already using the semiclassical Vlasov equation [7].

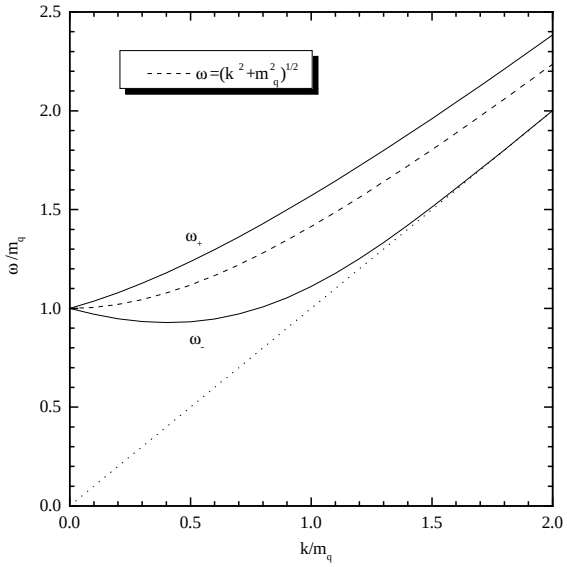

Figure 1. Quark dispersion relation in HTL approximation. Also shown are the free dispersion relations of massless (dotted line) and massive (dashed line) quarks.

modes have to be taken into account. The annihilation amplitude is related to the imaginary part of the photon self energy containing a quark loop by cutting rules [12]. According to the rules of the HTL method one has to use effective propagators and vertices as shown in Fig.2, if the photon energy and momentum are soft. The imaginary part of this diagram comes either from the pole of the effective quark propagator, corresponding to the dispersion relations of Fig.1, or from the the imaginary part of the HTL quark self energy contained in the resummed propagator (cut contribution). Therefore we have pole-pole, pole-cut, and cut-cut contributions to the dilepton production rate which is proportional to the imaginary part of the polarization tensor according to [13]

$$\frac{dN}{d^4x d^4p} = \frac{\alpha}{12\pi^4}\,\frac{1}{\mathrm{e}^{E/T}-1}\,\frac{\mathrm{Im}\,\Pi^{\mu}{}_{\mu}(P)}{M^2} \qquad (8)$$

with the QED fine-structure constant α and the invariant photon mass $M^2 \equiv P^2$. The pole-cut and cut-cut contributions involving external gluons, as can be seen by cutting the HTL quark

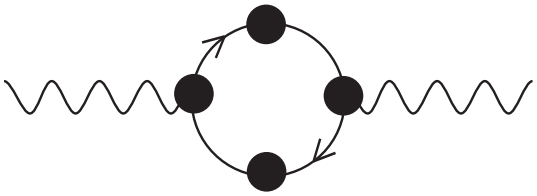

Figure 2. Photon self energy containing effective quark propagators and quark-photon vertices.

self energy, lead to a smooth contribution to the dilepton rate [11]. The pole-pole term, on the other hand, will cause sharp structures as we will discuss below.

Besides the dilepton production rates also temporal correlators of mesons follow from the diagram of Fig.2 [14]. These correlation functions of meson currents at the same space coordinate but different points in Euclidean time have been measured on the lattice in the deconfined phase (see e.g. Ref.[15]). A clear deviation from the free correlator, which is determined using only bare quark propagators and vertices in Fig.2 [16], has been found in particular in the pion channel [15]. This indicates the importance of quark interactions and medium effects in the QGP at temperatures close to the critical. Using HTL propagators and vertices as in Fig.2, medium effects, namely effective quark masses and Landau damping, are taken into account. It is interesting to study to what extend the HTL medium effects already explain the lattice results.

The spectral functions of the temporal correlators are proportional to the imaginary part of the quark loop diagram. The only difference compared to the photon self energy lies in the vertices describing the various mesonic channels. For example, in the pion channel the bare vertex is proportional to γ_5. In the vector channel, on the other hand, the bare vertex is proportional to γ_μ as in the dilepton case corresponding to Vector Meson Dominance.

In contrast to photons and vector mesons it is sufficient to consider a bare meson-quark vertex in Fig.2 for pseudo-scalar mesons. This is due to the fact that HTL vertices in the case of the

Yukawa theory lead only to higher order contributions and can be neglected therefore [17]. Since HTL vertices are complicated functions of the energy and momentum, we will discuss here only the spectral function of the pseudo-scalar temporal correlator. Actually the consideration of the effective vertex does not change the position of the Van Hove singularities, which are determined only by the minimum in the plasmino dispersion. Furthermore in the dilepton rate from the QGP the inclusion or neglect of the effective vertex does also not alter the magnitude of the rate significantly. This is in contrast to the dilepton rate from pion annihilation, where the consideration of the Ward identity reduced similar singularities in the rate strongly [18].

The spectral function of the pseudo-scalar correlator is given by

$$\sigma_{ps}(\omega,\boldsymbol{p}) = \frac{1}{\pi}\,\mathrm{Im}\;\chi_{ps}(\omega,\boldsymbol{p}), \tag{9}$$

where the correlation function in momentum space contains the quark loop according to

$$\chi_{ps}(\omega,\boldsymbol{p}) \;=\; 2N_c T\sum_n \int \frac{\mathrm{d}^3k}{(2\pi)^3}\;\mathrm{Tr}\Big[\gamma_5 S_{\mathrm{HTL}}(k_0,\boldsymbol{k}) \;\times\; \gamma_5 S_{\mathrm{HTL}}(\omega-k_0,\boldsymbol{p}-\boldsymbol{k})\Big]. \tag{10}$$

Here $N_c = 3$ is the number of colors, and the sum over n denotes the sum over the fermionic Matsubara frequencies $k_0 = (2n+1)i\pi T$.

The HTL resummed quark propagator is conveniently expressed by its spectral function ρ_{HTL}

$$S_F(k_0,\boldsymbol{k}) = -(\gamma_0\; k_0 - \boldsymbol{\gamma}\cdot\boldsymbol{k})\;\int_0^{1/T}\;\mathrm{d}\,\tau\,\mathrm{e}^{k_0\tau} \times\int_{-\infty}^{\infty}\mathrm{d}\omega\;\rho_{\mathrm{HTL}}(\omega,\boldsymbol{k})\;[1-n_F(\omega)]\;\mathrm{e}^{-\omega\tau}, \tag{11}$$

where $n_F(\omega) = 1/[1+\exp(\omega/T)]$ and

$$\rho_{\mathrm{HTL}}(k_0,\boldsymbol{k}) \;=\; \frac{1}{2}\,\rho_+(k_0,k)(\gamma_0 - i\,\hat{\boldsymbol{k}}\cdot\boldsymbol{\gamma}) \;+\; \frac{1}{2}\,\rho_-(k_0,k)(\gamma_0 + i\,\hat{\boldsymbol{k}}\cdot\boldsymbol{\gamma}) \tag{12}$$

with [11]

$$\rho_\pm(k_0,k) \;=\; \frac{k_0^2-k^2}{2m_q^2}[\delta(k_0-\omega_\pm)+\delta(k_0+\omega_\mp)] \;+\; \beta_\pm(k_0,k)\Theta(k^2-k_0^2). \tag{13}$$

Here the first part of (13) corresponds to the pole contribution of the HTL propagator. The second part, corresponding to the cut contribution from the imaginary part of the HTL quark self energy, is given by

$$\beta_\pm(k_0,k) \;=\; -\frac{m_q^2}{2}\,(\pm k_0 - k) \times\left\{\left[k(-k_0\pm k) + m_q^2\left(\pm 1 - \frac{\pm k_0 - k}{2k}\ln\frac{k+k_0}{k-k_0}\right)\right]^2 + \left[\frac{\pi}{2}m_q^2\frac{\pm k_0-k}{k}\right]^2\right\}^{-1}. \tag{14}$$

Combining (9) to (14) the spectral function of the pseudo-scalar correlator can be written as

$$\sigma_{\mathrm{ps}}(\omega,\boldsymbol{p}) = 2N_c(\mathrm{e}^{\omega/T}-1)\int\frac{\mathrm{d}^3k}{(2\pi)^3} \times\int_{-\infty}^{\infty}\mathrm{d}x\mathrm{d}x' n_F(x)n_F(x')\delta(\omega-x-x') \times\Big\{(1-\boldsymbol{q}\cdot\boldsymbol{k})[\rho_+(x,k)\rho_+(x',q)+\rho_-(x,k)\rho_-(x,q)] +(1+\boldsymbol{q}\cdot\boldsymbol{k})[\rho_+(x,k)\rho_-(x',q)+\rho_-(x,k)\rho_+(x,q)]\Big\}, \tag{15}$$

where $\boldsymbol{q} = \boldsymbol{p} - \boldsymbol{k}$. Considering only the pole-pole contribution originating from the first equation of (13) all the integrals in (15) can be done exactly. One finds

$$\sigma_{\mathrm{ps}}^{\mathrm{pp}}(\omega,\boldsymbol{p}=0) = \frac{N_c}{2\pi^2}\frac{(\mathrm{e}^{\omega/T}-1)}{m_q^4} \times\Big[n_F^2(\omega_+(k_1))\frac{\left(\omega_+^2(k_1)-k_1^2\right)^2k_1^2}{2|\omega_+'(k_1)|} +2\sum_{i=1}^{2}n_F(\omega_+(k_2^i))\big[1-n_F(\omega_-(k_2^i))\big] \times\frac{\left(\omega_-^2(k_2^i)-(k_2^i)^2\right)\left(\omega_+^2(k_2^i)-(k_2^i)^2\right)(k_2^i)^2}{|\omega_+'(k_2^i)-\omega_+'(k_2^i)|} +\sum_{i=1}^{2}n_F^2(\omega_-(k_3^i))\frac{\left(\omega_-^2(k_3^i)-(k_3^i)^2\right)^2(k_3^i)^2}{2|\omega_-'(k_3^i)|}\Big]. \tag{16}$$

Here $\omega_\pm(k)$ denote, as before, the quark dispersion relations for the ordinary quark (+) and the plasmino (-) branch, k_1 is the solution of $\omega - 2\omega_+(k_1) = 0$, k_2^i and k_3^i are the solutions

of $\omega-\omega_+(k_2^i)+\omega_-(k_2^i)=0$ and $\omega-2\omega_-(k_3^i)=0$, respectively. Note that for small momenta the last two equations can each have two solutions. Furthermore, $\omega'_\pm(k)\equiv(\mathrm{d}\omega_\pm(x)/\mathrm{d}x)|_{x=k}$.

Eq. (16) is shown in Fig.3 for $m_q/T=1$, i.e., $g=\sqrt{6}$. The first part of (16) corresponds to the annihilation of collective quark-antiquarks and sets in at the threshold $\omega\geq 2m_q$. For large energies this is the dominating contribution which approaches the result obtained from a bare quark propagator (crosses) for $\omega\gg m_q$. The second part corresponds to a transition from the upper quark branch to the lower plasmino branch. It starts at $\omega=0$ and terminates with an Van Hove singularity at $\omega=0.47\,m_q$, where the difference $\omega_+(k_2^i)-\omega_-(k_2^i)$ has a maximum due to the minimum in the plasmino dispersion. The third part describes the annihilation of plasminos and antiplasminos which starts at the threshold $\omega=1.86\,m_q$, where another Van Hove singularity occurs due the minimum of the plasmino branch $\omega_-(k_3^i)$. For larger momenta this contribution vanishes quickly due to the exponentially suppressed spectral strength of the plasmino branch. The singularities in (16) can be integrated leading to finite results for the temporal correlator [14]. Also in Fig.3 the smooth pole-cut and cut-cut contributions are shown. In particular the latter is suppressed by about an order of magnitude.

In the case of the spectral function of the vector correlator [14] and the dilepton production rate at zero momentum [11], for which an effective HTL vertex has to be used, the pole-pole and pole-cut contributions are similar (apart from some prefactors). In particular the Van Hove singularities are at the same positions. The cut-cut contribution, however, diverges for small ω covering up the low-energy Van Hove peak and leading to an infrared divergent vector correlator.

The temporal correlator follows from its spectral function by an energy integration [14]

$$G_{ps}(\tau) = \int_0^\infty \mathrm{d}\omega\,\sigma_{ps}(\omega,\boldsymbol{p}=0) \times \frac{\cosh(\omega(\tau-\beta/2))}{\sinh(\omega\beta/2)}, \qquad (17)$$

where $\beta=1/T$ and τ is restricted to the

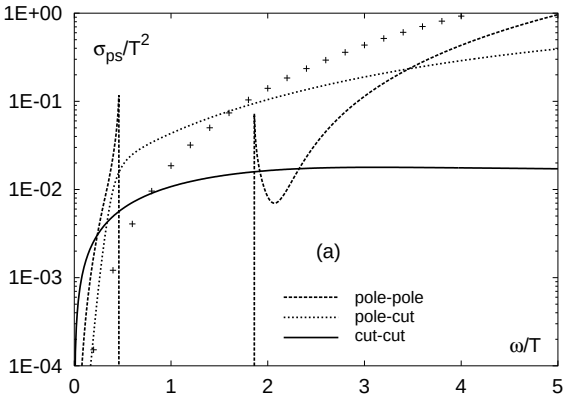

Figure 3. Pole-pole, pole-cut, and cut-cut contributions (solid lines) to the spectral function of the pseudo-scalar temporal correlator at $m_q/T=1$. The crosses indicate the free spectral function.

Euclidean time interval $[0,\beta]$. Using (17) together with (16) and the corresponding expressions for the pole-cut and the cut-cut contributions the temporal pseudo-scalar and vector correlators turn out be similar to the free correlation functions containing only bare quarks. This is caused by a competing effect of the pole-pole contribution and the pole-cut and cut-cut contributions. Whereas the pole-pole contribution reduces the spectral function due to the presence of the effective quark mass compared to the free spectral function, there is an enhancement due to the pole-cut and cut-cut contributions describing higher order diagrams involving external gluons. Surprisingly the two effects compensate each other in the temporal correlator almost completely. Hence the deviation from the free correlator, observed on the lattice, cannot be attributed to HTL medium effects [14].

3. Gluon condensate quark propagator

The problem connected with the above calculations relies in its perturbative nature. Since the coupling constant g is not small in realistic situations, the extrapolation to relativistic heavy ion collisions is questionable. Furthermore due

to collinear and magnetic divergences the convergence even of the HTL improved perturbative series at finite temperature is upset at least for low mass $M \simeq g^2 T$ dileptons [19].

In Ref.[20] another effective quark propagator has been constructed by taking into account the gluon condensate measured in lattice QCD calculations above the phase transition. In this way non-perturbative effects are included, which allow to study realistic temperatures addressed on the lattice. For this purpose we calculate the quark self energy from a one-loop diagram using a non-perturbative gluon propagator that contains the gluon condensate analogously to the zero temperature case [21]. Of course, the approach is a purely phenomenological combination of Green functions with lattice results. The effective quark propagator can then be written as in (6) and (7) with

$$\begin{aligned} a &= -\frac{g^2}{6}\frac{1}{K^6}\left[\left(\frac{1}{3}k^2 - \frac{5}{3}k_0^2\right)\langle \mathcal{E}^2\rangle_T \right. \\ &\quad \left. -\left(\frac{1}{5}k^2 - k_0^2\right)\langle \mathcal{B}^2\rangle_T\right], \\ b &= -\frac{4}{9}g^2\frac{k_0}{K^6}\left[k_0^2\langle \mathcal{E}^2\rangle_T + \frac{1}{5}k^2\langle \mathcal{B}^2\rangle_T\right], \end{aligned} \qquad (18)$$

where the in-medium chromoelectric, $\langle \mathcal{E}^2\rangle_T$, and chromomagnetic condensates, $\langle \mathcal{B}^2\rangle_T$, are taken from lattice calculations [22].

In Fig.4 the dispersion relations following from the poles of this propagators are shown at $T = 2T_c$ [20]. The important point here is that, although the HTL resummed and the gluon condensate quark propagators are completely different, the dispersion relations show the very same behaviour. In particular we observe again the minimum in the plasmino branch. Therefore we expect again Van Hove singularities in the dilepton rate following from this quark propagator. In a first step we neglected an effective quark-photon vertex, related to the gluon condensate quark propagator by Ward identities [23]. However, as we discussed above, this will not change the existence and positions of Van Hove singularities following solely from the quark dispersion relations. In Fig. 5 the dilepton production rate at zero photon momentum versus the invariant photon mass M from this investigation [24] is shown for different temperatures. The interpretation of the various curves is identical with the one in the last section. However, in this case no pole-cut and cut-cut contribution are present as the quark self energy containing the gluon condensate has no imaginary part [20].

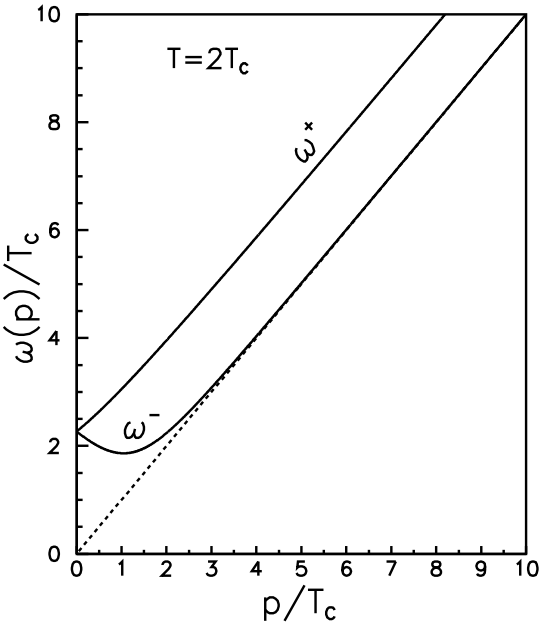

Figure 4. Quark dispersion relations according to the gluon condensate quark propagator at $T = 2T_c$.

4. General quark dispersion relations

The two completely different approximations for the quark propagator, discussed in the last two sections, lead to the same qualitative behaviour of the dispersion relations. Hence one may speculate that the dispersion relations shown in Fig.1 and Fig.4 are a consequence of the most general full propagator for massless fermions at finite temperature. Analyzing the most general expression for the in-medium fermion propagator (6) and (7) one can show the following general properties of the dispersion relations [25]: (1) there are always two branches; (2) both branches start at the same

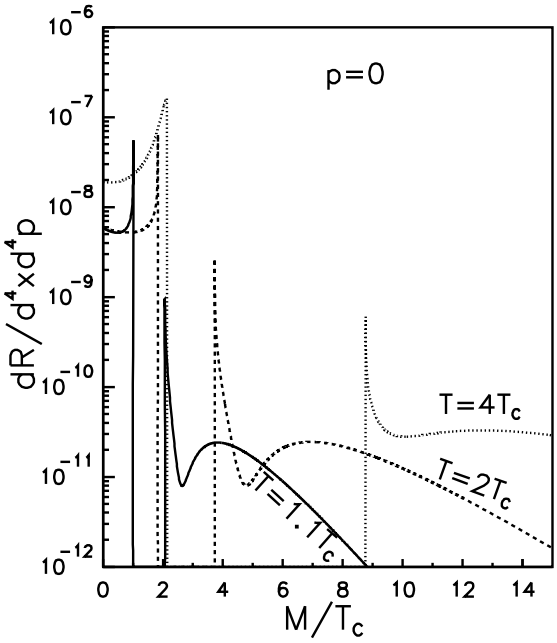

Figure 5. Dilepton production rate at zero photon momentum versus the invariant photon mass M following from the gluon condensate quark propagator.

energy, i.e. effective fermion mass, at zero momentum; (3) the both branches have an opposite slope at zero momentum; (4) the branch corresponding to the usual fermion approaches the free dispersion relation, $\omega = k$, for large momenta k. Assuming that the plasmino branch also approaches the free dispersion at large momenta, as it does in the two independent examples discussed above, the plasmino branch must always possess a minimum. So far this assumption has not been proven. Maybe future lattice calculations might be capable of investigating the quark dispersion relations [26]. However, it appears to be reasonable that the plasmino minimum is a general feature leading to Van Hove singularities in the dilepton production rate and mesonic temporal correlators.

5. Consequences for relativistic heavy ion collisions

Now the important question is whether the Van Hove singularities in the QGP can be observed in relativistic heavy ion collisions. One possibility would be to look at the low-mass dilepton spectrum, which has been investigated already at SPS energies [27]. Here no sign for interesting structures due to Van Hove singularities has been found. However, hydrodynamic simulations [28] show that the QGP contribution, if there is a QGP phase at all as indicated at SPS [29], are suppressed at least by an order of magnitude compared to the hadronic contributions. This situation will change at RHIC and LHC, where the QGP contribution should dominate the thermal emission from the fireball. If low-mass dileptons should be investigated at RHIC or LHC, interesting structures coming from the Van Hove peaks and the gap in the dilepton rate might appear. From a comparison of the equation of state found in lattice calculations and quasiparticle models [30] effective quark masses of the order 500 MeV are expected. Therefore the structures may show up at invariant masses below about 1 GeV.

To what extent these distinct structures will survive in heavy ion collisions depends on how much of it will be covered and smeared out by higher order effects, e.g. bremsstrahlung and damping. Also finite momenta [24,31] and the space-time evolution of the fireball will wash out the structures to some degree. These effects are an interesting subject for future investigations. Anyway, if a non-trivial structure should be observed in the low-mass dilepton spectrum it would provide an unique signal for the QGP formation, since one does not expect a similar signal from the hadronic phase. Due to in-medium collisions between hadrons the structures from the hadronic phase such as the ρ-peak are washed out [32]. Hence structures in the low mass dilepton spectrum due to Van Hove singularities would not only indicate a deconfined phase, but also the existence of collective quark modes in the QGP.

6. Conclusions

The quark dispersion relations in the QGP have been studied using two different approximations for the quark propagator. First the HTL method, which is based on the resummation of the perturbative quark self energy obtained in the high tem-

perature limit has been adopted. Secondly the gluon condensate measured on the lattice above the critical temperature has been included in the effective quark propagator. The poles of the effective quark propagators, following from these completely different approaches, determine quark dispersion relations which show the same behaviour. In both approaches two branches, of which one shows a minimum, namely the plasmino branch, have been found. There are strong indications that this is a general feature of massless fermions at finite temperature.

The minimum in the plasmino branch leads to a vanishing group velocity of the plasma modes and therefore to a diverging density of states in the low-mass dilepton production rate and in the spectral function of mesonic correlators. Therefore Van Hove singularities appear in these quantities. The dilepton production might serve as a promising signature for the QGP formation in relativistic heavy ion collisions. Whether these Van Hove singularities can be observed in the dilepton spectrum from a dynamical QGP, produced possibly in the fireball of a nucleus-nucleus collision, is an open question. Anyway it will be worthwhile to look for non-trivial structures, indicating the existence of deconfined, collective quark modes, in the low-mass dilepton spectrum at RHC and LHC.

The meson correlation functions, on the other hand, can be compared to lattice calculations, which allows to extract informations on the non-perturbative nature of the QGP. Future QCD lattice calculations might be able to investigate directly the quark dispersion relations and the spectral functions of the mesonic correlators [33], which contain much more informations than the correlators themselves. Summarizing, the verification of Van Hove singularities in the QGP experimentally as well as on the lattice will be an interesting challenge.

ACKNOWLEDGMENTS

Most of the results presented here have been obtained in collaboration with F. Karsch, M. Mustafa, A. Peshier, and A. Schäfer.

REFERENCES

1. L. Van Hove, Phys. Rev. 89 (1953) 1189.
2. N.W. Ashcroft and N.D. Mermin, *Solid State Physics* (Saunders College, Philadelphia, 1976).
3. R.S. Markiewicz, J. Phys. Chem. Sol. 58 (1997) 1179.
4. E. Braaten and R.D. Pisarski, Nucl. Phys. B 337 (1990) 569.
5. J.A. Lopez, J.C. Parikh, and P.J. Siemens, Texas A& M preprint, 1985 (unpublished).
6. V.V. Klimov, Sov. Phys. JETP 55 (1982) 199; H.A. Weldon, Phys. Rev. D 26 (1982) 1394.
7. V.P Silin, Sov. Phys. JETP 11 (1960) 1136.
8. E. Braaten and R.D. Pisarski, Phys. Rev. D 42 (1990) 2156.
9. M.H. Thoma, in: *Quark-Gluon Plasma 2*, ed. R.C. Hwa (World Scientific, Singapore, 1995), p.51; M.H. Thoma, Nucl. Phys. A 638 (1998) 317c.
10. H.A. Weldon, Phys. Rev. D 26 (1982) 2789.
11. E. Braaten, R.D. Pisarski, and T.C. Yuan, Phys. Rev. Lett. **64**, (1990) 224.
12. H.A. Weldon, Phys. Rev. D 28 (1982) 2007.
13. C. Gale and J.I. Kapusta, Nucl. Phys. B 357 (1991) 65.
14. F. Karsch, M. Mustafa, and M.H. Thoma, hep-ph/0007093.
15. G. Boyd, S. Gupta, F. Karsch, and E. Laermann, Z. Phys. C 64 (1994) 331.
16. W. Florkowski and B. Friman, Z. Phys. A 347 (1994) 271.
17. M.H. Thoma, Z. Phys. C 66 (1995) 491.
18. C.L. Korpa and S. Pratt, Phys. Rev. Lett. 64 (1991) 1502.
19. P. Aurenche, F. Gelis and H. Zaraket, Phys. Rev. D 61 (2000) 116001.
20. F.A. Schäfer and M. H. Thoma, Phys. Lett. B 451 (1999) 195.
21. M.J. Lavelle and M. Schaden, Phys. Lett. B 208 (1988) 297.
22. G. Boyd *et al.*, Nucl. Phys. B 469 (1996) 419.
23. M. G. Mustafa, A. Schäfer and M. H. Thoma, Phys. Lett. B 472 (2000) 402.
24. M. G. Mustafa, A. Schäfer and M. H. Thoma, Phys. Rev. C 61 (2000) 024902.
25. A. Peshier and M.H. Thoma, Phys. Rev. Lett.

84 (2000) 841.
26. F. Karsch, private communication.
27. G. Agakichiev et al., CERES collaboration, Phys. Lett. B 422 (1998) 405.
28. J. Sollfrank et al., Phys. Rev. C 55 (1997) 392.
29. U.Heinz and M. Jacobs, nucl-th/0002042.
30. A. Peshier, B. Kämpfer, O.P. Pavlenko, and G. Soff, Phys. Rev. D 54 (1996) 2399.
31. S.M.H. Wong, Z. Phys. C 53 (1992) 465.
32. R. Rapp and J. Wambach, Eur. Phys. J. A 6 (1999) 415.
33. I. Wetzorke and F. Karsch, hep-lat/0008008.